Flux-gradient relation and atmospheric wind profiles — an exploration using WRF and lidars

Santos, Pedro; Peña, Alfredo; Mann, Jakob

Published in:
Journal of Physics: Conference Series

Link to article, DOI:
10.1088/1742-6596/1618/3/032032

Publication date:
2020

Document Version
Publisher's PDF, also known as Version of record

Flux-gradient relation and atmospheric wind profiles — an exploration using WRF and lidars

Flux-gradient relation and atmospheric wind profiles – an exploration using WRF and lidars

Pedro Santos, Alfredo Peña and Jakob Mann
DTU Wind Energy, Technical University of Denmark, Roskilde, Denmark
E-mail: paas@dtu.dk

Abstract. A common closure for the planetary boundary layer in numerical weather models assumes a direct relation between turbulent fluxes and the mean wind vertical gradient, i.e., the flux-gradient relation or K-theory. This assumption implies that the angle β between the momentum stress vector and the mean gradient of the velocity vector are aligned, i.e., $\beta = 0°$. This is not what we observe from measurements. We quantify the misalignment of β in offshore conditions using measurements from a long-range Doppler profiling lidar and numerical simulations from the New European Wind Atlas mesoscale model output. We compare vertical profiles of wind speed, wind direction, momentum fluxes, and β up to 500 m, hence covering the rotor areas of modern offshore wind turbines and beyond. The results show that $\beta \approx -18°$ on average, with a lower, but still non-zero, value under stable stability conditions, $\approx -7°$. We illustrate that the simulations describe well the mean wind speed and momentum fluxes within the observed levels, but the characterization of wind turning effects could be improved.

1. Introduction

Current wind turbine rotors operate under vertical wind shear and wind veer conditions over a portion of the planetary boundary layer (PBL), which can surpass the atmospheric surface layer (ASL) or "constant-flux" layer by hundreds of meters, depending on the atmospheric stability and turbulence conditions. The Monin-Obukhov similarity theory (MOST) is used as the standard description of the ASL on flat and homogeneous conditions, e.g., far offshore [1]. However, our comprehension of wind climatology and turbulence above the ASL has to be improved in order to refine the capabilities of numerical models such as the Weather Research and Forecast (WRF) model to simulate the atmosphere.

Recent studies took advantage of long-range Doppler profiling wind lidars by probing the atmosphere up to $\approx$ 1 km to gain insight of the wind climatology beyond the ASL, e.g., by characterizing the Weibull parameters [2], and by comparison with mean wind profiles from WRF PBL schemes [3]. Regarding the measurement of second-order moments by ground-based lidars, a variety of methods have been developed [4] and the lidar limitations quantified, such as the turbulence attenuation due to a spatial averaging by the probe volume [5]. Hence, there is an opportunity to better evaluate numerical models and parametrizations of the PBL with wind lidars.

Some PBL parametrizations in WRF consider the flux-gradient relation or K-theory,

$$\langle u'w' \rangle = -K_m \frac{\partial U}{\partial z} \quad \text{and} \tag{1}$$

$$\langle v'w' \rangle = -K_m \frac{\partial V}{\partial z}, \tag{2}$$

where U and V are the two horizontal mean wind components aligned with the geographical coordinates, u' and v' are fluctuations around both means and $\langle \quad \rangle$ represents the ensemble mean.

Each PBL scheme can have a different formulation for the eddy difusivity K_m, but the flux-gradient assumption tends to break down as the influence of the Coriolis force grows, resulting in a misalignment between the momentum stress vector $(-\langle u'w' \rangle, -\langle v'w' \rangle)$ and the mean wind vector (U, V). A departure from the K-theory can be observed with the misalignment between the stress vector and the vertical gradient of the mean wind vector $(\partial U/\partial z, \partial V/\partial z)$. Those angles are herein defined as α and β, respectively, illustrated in figure 1 and defined as,

$$\alpha = \text{atan2}(U, V) - \text{atan2}(-\langle u'w' \rangle, -\langle v'w' \rangle) \quad \text{and} \tag{3}$$

$$\beta = \text{atan2}\left(\frac{\partial U}{\partial z}, \frac{\partial V}{\partial z}\right) - \text{atan2}(-\langle u'w' \rangle, -\langle v'w' \rangle). \tag{4}$$

Note that when numerical models consider the flux-gradient relation, $\beta = 0°$. Previous work has shown non-zero vertical profiles of β, derived using observations from a short-range wind lidar up to 200 m at the onshore but rather flat site of Høvsøre, Denmark [6]. Nonetheless, at Høvsøre there are some surface heterogeneity, which can impact the results.

In this work, we compute mean wind and momentum flux profiles offshore with both wind lidar measurements and the WRF output from the New European Wind Atlas (NEWA [1]), which uses the K-theory, hereafter NEWA-WRF. The aim is to compare the vertical profiles of α and β between the measurements and the model output. Furthermore, we quantify the behavior of β as well as the wind direction bias from WRF with a proxy of atmospheric stability, the latter being regarded as a long-standing issue in numerical weather models [7]. The analysis intends to assess the validity of the eddy diffusivity approach and discusses the consequences of this in, e.g., mesoscale models.

2. Methodology

2.1. Site and measurements

We present results from a one-year campaign at the FINO3 offshore research platform (55°11.7′N, 7°9.5′E), where a long-range pulsed wind lidar (WindCube WLS70) was deployed on the deck of the platform, 24.5 m above the mean sea level (amsl), next to a fully instrumented 100-m meteorological mast. All heights are referred to amsl hereafter unless otherwise stated. A preliminary study detailed the instrumentation and showed the agreement between wind lidar measurements and a cup anemometer for the first nine months of the campaign [8].

The WLS70 wind lidar measured the radial wind speed v_r at the four cardinal directions, namely $v_{r,N}, v_{r,S}, v_{r,E}, v_{r,W}$, with a half opening angle from the vertical ϕ =14.67°. The wind vector is derived every ≈10 s from 100 to 2000 m above the lidar with a 50 m vertical resolution. The lidar probe length is ≈ 75 m.

For this study, we select the entire lidar measurement period, between 1 September 2013 and 1 October 2014. During this period, we use concurrent 10-min measurements from a cup anemometer at 106 m to verify the wind lidar measurements, as well as air temperature at 30 m and water temperature from a nearby meteorological buoy, which will be used for a proxy of the atmospheric stability.

[1] https://map.neweuropeanwindatlas.eu/

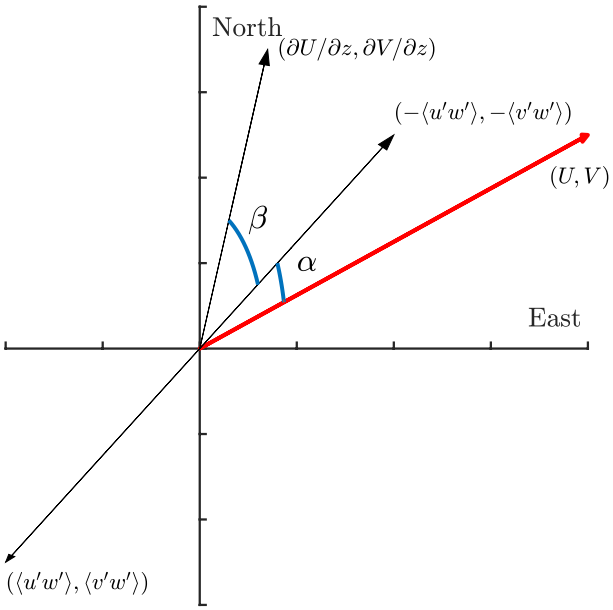

Figure 1. Illustration of α and β in respect to the stress vector $(-\langle u'w'\rangle, -\langle v'w'\rangle)$.

2.2. Data selection and filtering

The lidar's carrier-to-noise ratio (CNR) is an indication of the quality of v_r estimation. A CNR lower limit of -29 dB is used to filter radial wind speeds at all heights up to 500 m, so only fully available profiles up to this height are selected for the analysis. We choose -29 dB as threshold since this value gives an unbiased estimation of the wind climatology [9] and will also provide more valid profiles for robust statistics.

Along with the CNR threshold, a further filter was applied. We compute the radial wind speed median ($\tilde{v_r}$) for each range gate and azimuth angle. To calculate $\langle v_r \rangle$ and $\sigma^2(v_r)$ the criterion excludes outliers when $|v_r - \tilde{v_r}| > 6\,\mathrm{m\,s^{-1}}$. This procedure allows to include periods with rain, which are usually compromised due to second returns from clouds and spikes in the time series.

Lidar measurements at 300 m had a consistent negative bias due to an interference in the laser signal, which was also observed in a previous campaign with this equipment [3]. The problem was solved after the FINO3 campaign by replacing the laser source. Hence, this measurement height was removed in our analysis.

We calculate 30-min ensemble averages throughout this work. Table 1 shows the quantity of selected data from the one-year measurement campaign. Three consecutive and valid 10-min periods are considered as the reference dataset. From this sample of 10926 30-min periods, we apply the filters and reach 76.2% of valid full profiles up to 500 m. The concurrent temperature measurements will be used to calculate the potential temperature gradient ($\Delta\Theta$) almost without loosing any additional data.

For the lidar wind speed verification against the cup anemometer, there are 65.6% of the profiles available. Results agree with preliminary studies [8] showing an excellent agreement for wind speed correlation between the cup at 106 m and the first wind lidar level at 124.5 m, with a coefficient of determination $R^2 = 0.99$. The wind lidar derived wind direction and a vane at 100 m on the meteorological mast shows a wind direction offset of –11.7° [8], which we apply in our computations to correct for a potential lidar offset with the north.

Data Selection	30-min periods	% of total
Full 30-min profiles (30-min lidar)	8323 (10926)	76.2% (100%)
Concurrent full profiles & $\Delta\Theta$	8320	76.2%
Concurrent lidar & cup 106 m	7173	65.6%

Table 1. Data selected from all valid lidar measurements (CNR≥ -29 dB) for the period between 01 September 2013 to 01 October 2014.

2.3. Lidar-derived momentum fluxes

The computation is based on the difference between the variance of opposing lidar beams, originally proposed by [10] and more recently applied by [5],

$$\begin{pmatrix} \langle u'w' \rangle \\ \langle v'w' \rangle \end{pmatrix} = \frac{1}{2\sin 2\phi} \begin{pmatrix} \cos\delta & -\sin\delta \\ \sin\delta & \cos\delta \end{pmatrix} \begin{pmatrix} \sigma^2(v_{r,E}) - \sigma^2(v_{r,W}) \\ \sigma^2(v_{r,N}) - \sigma^2(v_{r,S}) \end{pmatrix}, \tag{5}$$

where δ is the angle between the north and the $v_{r,N}$ laser beam.

For this method, statistical horizontal homogeneity is required in order to combine radial wind speeds from distinct points in space and obtain turbulence statistics. Therefore, vertical profiles of momentum fluxes up to 500 m are better characterized by Eq. 5 in offshore conditions, since it requires in theory a homogeneous upstream fetch.

2.4. Momentum fluxes estimated from the NEWA-WRF outputs

NEWA-WRF outputs are available for all EU countries, including a 100 km offshore fetch plus all of the the Baltic and the North Sea, and covers 30 yr (1989–2018). The dynamic forcing used was the 0.3° resolution ERA5 reanalysis. The detailed description of the model is given in [11] with a sensitivity analysis that compares the performance of several PBL schemes using meteorological masts, i.a., FINO3. Results showed that a modified version of the Mellor-Yamada Nakanishi-Niino (MYNN) scheme [12] provided the minimum wind speed bias in most validation sites [11].

The NEWA-WRF final product, i.e., a subset of the full model output, offers a 30-min time series over the entire 30-yr period, with a 3-km resolution and seven vertical levels at 50, 75, 100, 150, 200, 250, and 500 m. To extract the time series at FINO3 from the model output over the spatial domain, a linear interpolation was performed using the nearest neighbor grid cells.

The MYNN level 2 (MYNN2) is a local scheme, i.e., fluxes are derived from local quantities, based on the prognostic turbulent kinetic energy (TKE) scheme from Mellor-Yamada [13]. MYNN2 applies the flux-gradient relation as expressed in Eqns. (1) and (2), where the eddy difusivity K_m is given by,

$$K_m = lqS, \tag{6}$$

where l is a master length scale, $q = \sqrt{2e}$ with e being the TKE and S is a non-dimensional eddy diffusivity coefficient, which accounts for atmospheric stability. Since l is not available in the NEWA-WRF output, we derive it following the MYNN2 approach [12].

3. Results

3.1. Lidar and NEWA-WRF wind climatology

Figure 2 shows the concurrent wind roses measured by the wind lidar at 124.5 m and modeled by WRF at 100 m. The model has a good description, on average, of the wind speed and direction distribution, but its possible to observe a general underestimation of the wind speed. Some

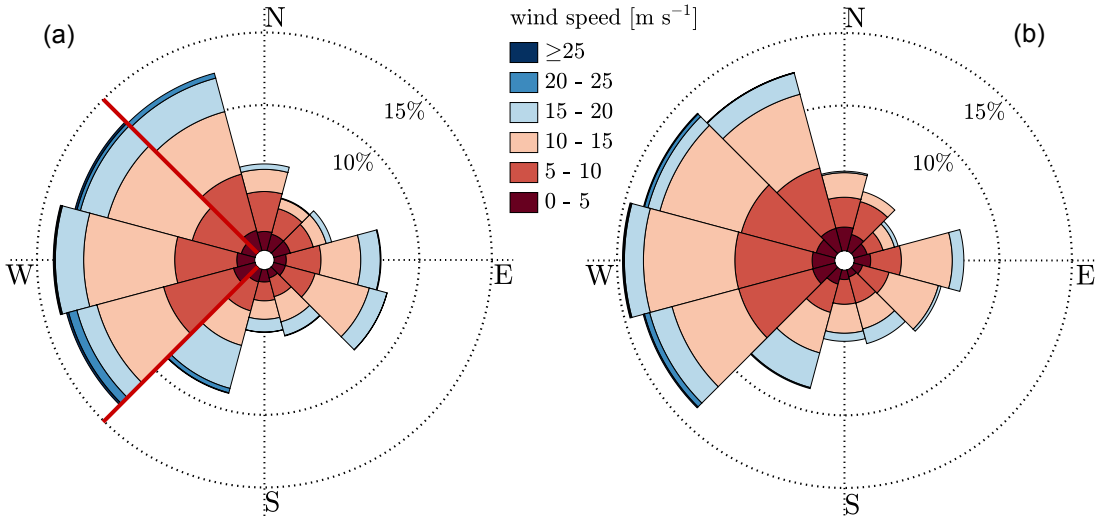

Figure 2. Wind rose measured by the wind lidar at 124.5 m (a) and concurrently simulated by NEWA-WRF at 100 m (b). The red lines in (a) show the westerly sector ($270° \pm 45°$) selected for the analysis.

differences can also be seen in some wind direction bins, which already indicates the presence of a persistent wind direction bias.

Westerly winds are prevalent at FINO3. Therefore we select for the analysis the wind directions $270° \pm 45°$ based on the measurements from the first level of the wind lidar. The selected sector is shown between the red lines in Figure 2a and represent $\approx 50\%$ of the total distribution. The size of the selected sector does not have a major impact on the vertical profiles presented below.

3.2. Vertical profiles

Figure 3 shows the derived vertical profiles computed from the wind lidar measurements (blue lines) and concurrent WRF (red lines) simulations for the westerly sector. For each level the shaded area represents the standard error given by $\pm\sigma/\sqrt{N}$, where σ is the standard deviation and N the number of observations. The mean WRF's PBL height is 925 m, but during stable stratification the profiles can be close to the PBL top.

From the U and V profiles (Fig. 3a), it is clear that WRF underestimates the wind turning in the PBL. This is a well-known issue from numerical weather models [14] and it was already observed with long-range lidars in other sites [15]. It is worth noticing that this type of pulsed Doppler wind lidar is ideal to quantify the wind veer, since it is capable to measure all heights at once.

The momentum flux profiles (Fig. 3b) behave as expected, with $\langle v'w' \rangle$ close to zero for the westerly sector and $\langle u'w' \rangle$ decreasing (in magnitude) with height almost linearly. There is nonetheless a mismatch for the $\langle u'w' \rangle$ profile, that can be caused either by WRF or the lidar (or both). The wind speed vertical gradients are similar both in the model and observations (not shown). Therefore, if the bias originates from the simulations, then the estimate of K_m is under suspicion. On the other hand, the lidar-derived momentum fluxes are most probably attenuated due to spatial averaging along the line-of-sight, i.e., probe-volume effects. In a preliminary estimation of the lidar filtering effect under neutral conditions and considering that turbulence can be described by the Mann model [16] with a length scale ≈ 50 m, we find a 25% decrease

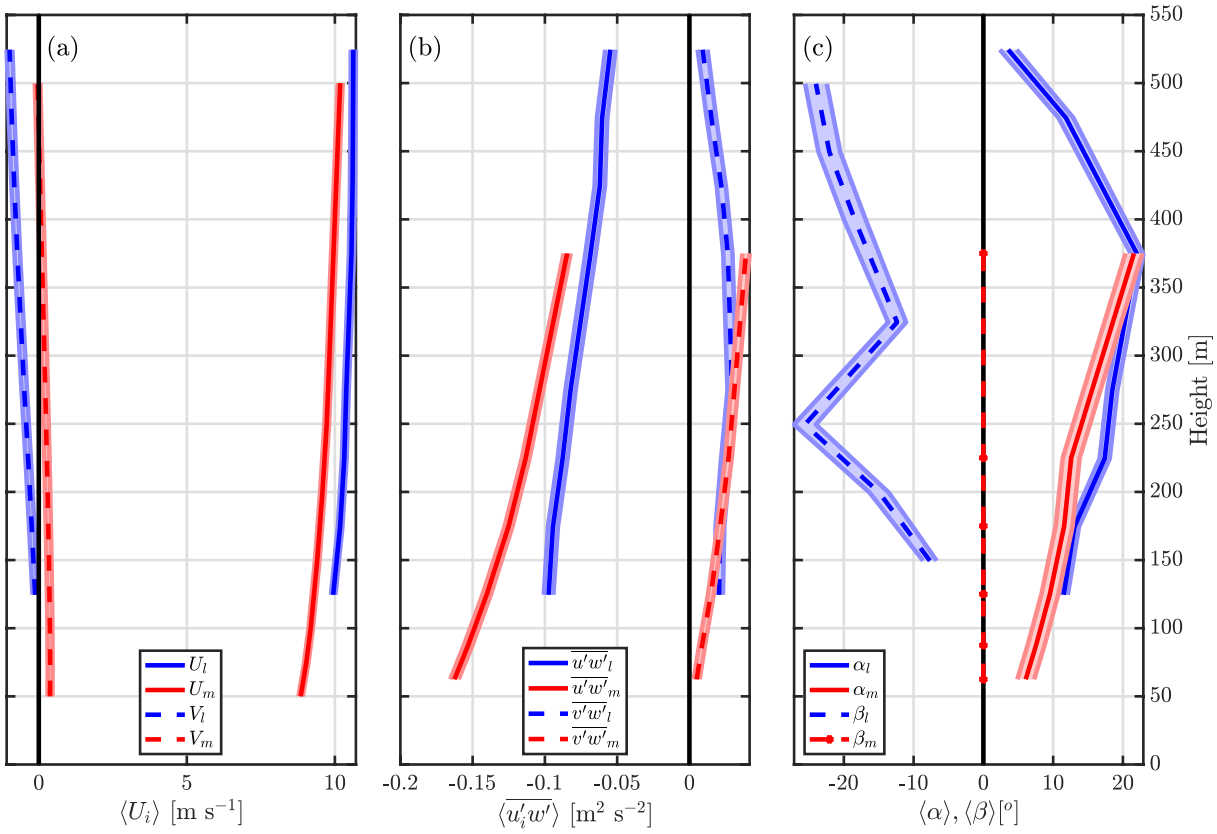

Figure 3. Mean vertical profiles of horizontal wind components (a), momentum fluxes (b) and turning angles (c) for westerly winds ($270° \pm 45°$). Blue lines are wind lidar (subscript l) and red lines are NEWA-WRF (subscript m). Total number of 30-min profiles is 3343. Shaded areas denote associated standard errors of the mean.

in the momentum flux due to filtering. This would account for almost all the $\langle u'w' \rangle$ mismatch above the ASL.

As expected from previous large-eddy simulations (LESs) [6], $\langle \alpha \rangle$ increases with height (Fig. 3c). Furthermore, WRF results agree well with the derived lidar measurements for this particular wind sector. However, other wind direction sectors do not show such an agreement. Additionally, one must notice that the agreement on $\langle \alpha \rangle$ can be due to a combination of biases in both wind direction and momentum fluxes.

The most evident mismatch between the measurements and simulation results is for $\langle \beta \rangle$, as expected, since MYNN2 assumes this is zero (Fig. 3c). The mean misalignment for all heights is $\langle \beta \rangle \approx -18°$ and is not much sensitive to CNR threshold or to the size of the westerly sector. The β profiles and, hence, the flux-gradient relation are sensitive to the vertical gradients of mean wind. So a reasonable assumption is that MYNN2 (and other local TKE schemes) would show a better performance under stable conditions, i.e., where the vertical gradients are large [17].

3.3. Effect of atmospheric stability on β and wind turning

We compute the potential temperature gradient $\Delta\Theta = \Theta_{30\,\mathrm{m}} - \Theta_{buoy}$, using concurrent air temperature measurements at 30 m and water measurements from the nearby meteorological buoy. Since there is no high frequency sonic anemometer data at FINO3, $\Delta\Theta$ is used as a simple

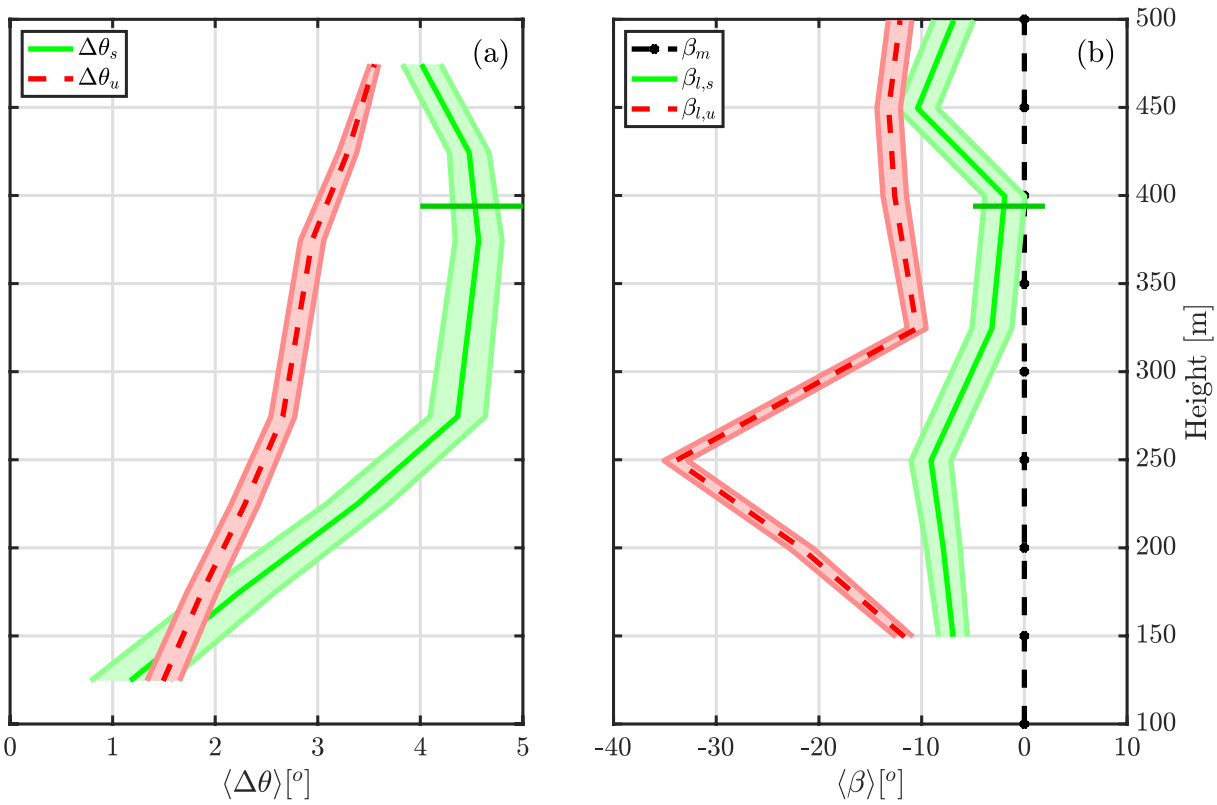

Figure 4. Vertical profiles of wind direction bias between the wind lidar observations and NEWA-WRF simulations (a) and β (b) for unstable (red, dotted lines) and stable (green, full lines) conditions. The black $\beta = 0°$ profile is assumed by NEWA-WRF. Shaded areas denote associated standard errors of the mean. The horizontal line represents WRF's mean PBL height for stable conditions.

proxy for atmospheric stability. Hence, $\Delta\Theta < 0\,\mathrm{K}$ is used to identify unstable conditions and $\Delta\Theta > 0\,\mathrm{K}$ for stable conditions.

Figure 4 shows the vertical profiles of the wind direction bias between the wind lidar and WRF $\langle\Delta\theta\rangle = \langle\theta_l - \theta_m\rangle$ (Fig. 4a) and the $\langle\beta\rangle$ profiles (Fig. 4b) for stable and unstable conditions. According to our atmospheric stability criterion, unstable conditions are predominant at FINO3 and represent 85.5% of profiles. The mean WRF PBL height for unstable conditions is 993 m, hence not shown. NEWA-WRF also outputs the inverse Obukhov length L^{-1}. When comparing the sign of L^{-1} with the sign of the measured potential temperature gradient we find that 76% of the observed stable profiles are indeed simulated as such whereas 90% of the observed unstable profiles are also simulated as such by the model.

Results from $\langle\Delta\theta\rangle$ profiles show that WRF consistently underestimates the wind direction veer, with a higher bias for stable conditions, as expected. This is in line with previous findings, where PBL schemes tend to produce more mixing compared to what is observed under stable conditions, which leads to an underestimation of both wind shear and veer [15]. The vertical profiles of $\langle\beta\rangle$ also behave as expected, with a lower value $\approx -7°$ on average under stable conditions, and approaching zero closer to the PBL top also under stable stratification. Although with fluctuations, $\langle\beta\rangle$ values are always larger under unstable compared to stable conditions.

4. Conclusions

We present novel measurements performed with a wind lidar on the FINO3 offshore platform that show the misalignment between the stress vector and the vertical gradient of the mean wind vector up to 500 m in the marine PBL. This cannot be simulated with current setups of numerical weather models, such as that used for the NEWA project. Results show that the derived vertical profiles of the momentum flux from a pulsed wind lidar are, apart from the mentioned misalignment, in agreement with those derived from the NEWA-WRF outputs. In particular, the turning of the stress vector relative to the mean wind vector derived from the mesoscale outputs agrees very well with the measurements.

Profiles of momentum transport with the spatial and temporal resolution presented herein can potentially add value to better describe the entrainment process of mean kinetic energy, with the evaluation of $-\langle U_i \rangle \langle u_i' w' \rangle$ in and above large offshore wind farms. Up to now, this application was mainly studied using LESs [18].

The performance of other PBL schemes to describe vertical momentum transfer, such as the non-local Yonsei University (YSU) scheme, also deserves further attention. For more details on the performance of YSU, MYNN2 and other PBL schemes, refer to the work by Peña *et al* in these proceedings. Further work can extend this analysis to other locations where sonic anemometers are present, allowing to quantify the lidar turbulence attenuation due to spatial averaging.

References

[1] Businger J A, Wyngaard J C, Izumi Y and Bradley E F 1971 *Journal of the Atmospheric Sciences* **28** 181–189
[2] Gryning S E, Floors R, Peña A, Batchvarova E and Brümmer B 2016 *Boundary-Layer Meteorology* **159** 329–348
[3] Floors R, Vincent C L, Gryning S, Peña A and Batchvarova E 2013 *Boundary-Layer Meteorology* **147** 469–491
[4] Sathe A and Mann J 2013 *Atmospheric Measurement Techniques* **6** 3147–3167
[5] Mann J, Peña A, Bingöl F, Wagner R and Courtney M S 2010 *Journal of Atmospheric and Oceanic Technology* **27** 959–976
[6] Berg J, Mann J and Patton E G 2013 *Journal of Atmospheric and Oceanic Technology* **30** 1961–1969
[7] Simpson I R, Bacmeister J T, Sandu I and Rodwell M J 2018 *Journal of Climate* **31** 491–513
[8] Peña A, Gryning S E and Floors R 2015 *Meteorologische Zeitschrift* **24** 581–589
[9] Gryning S E and Floors R 2019 *Sensors (Basel, Switzerland)* **19** 592
[10] Eberhard W L, Cupp R E and Healy K R 1989 *Journal of Atmospheric and Oceanic Technology* **6** 809–819
[11] Hahmann A N, Sile T, Witha B, Davis N N, Dörenkämper M, Ezber Y, García-Bustamante E, González Rouco J F, Navarro J, Olsen B T and Söderberg S 2020 *Geoscientific Model Development Discussions* **2020** 1–33
[12] Nakanishi M and Niino H 2009 *Journal of the Meteorological Society of Japan. Ser. II* **87** 895–912
[13] Mellor G L and Yamada T 1982 *Reviews of Geophysics* **20** 851–875
[14] Brown A R, Beljaars A C M, Hersbach H, Hollingsworth A, Miller M and Vasiljevic D 2005 *Quarterly Journal of the Royal Meteorological Society* **131** 1233–1250
[15] Peña A, Gryning S E and Floors R 2014 *Journal of Physics: Conference Series* **524** 012118
[16] Mann J 1994 *Journal of Fluid Mechanics* **273** 141–168
[17] Shin H H and Hong S Y 2011 *Boundary-Layer Meteorology* **139** 261–281
[18] Andersen S J, Sørensen J N and Mikkelsen R F 2017 *Philosophical Transactions of the Royal Society A: Mathematical, Physical and Engineering Sciences* **375** 20160107